12th International Symposium on Turbulence and Shear Flow Phenomena (TSFP12)
Osaka, Japan (Online), July 19–22, 2022

MULTI-STRUCTURE TURBULENCE IN A BOUNDARY LAYER WITH A UNIFORMLY SHEARED FREE STREAM

Curtis Livingston
Department of Mechanical Engineering
University of Ottawa
Ottawa, ON K1N 6N5, Canada
curtis.livingston25@gmail.com

Stavros Tavoularis
Department of Mechanical Engineering
University of Ottawa
Ottawa, ON K1N 6N5, Canada
stavros.tavoularis@uottawa.ca

ABSTRACT

A turbulent boundary layer (TBL), generated in a water tunnel, extended to an anisotropic turbulent "free stream", consisting of a uniformly sheared flow (USF) with a mean shear that was in the opposite direction to that in the TBL. Measurements of the fluctuating velocity were taken with the use of hot-film anemometry, laser Doppler velocimetry and particle image velocimetry. On either side of the TBL edge, defined as the location of maximum velocity, the turbulence relaxed to its canonical structures in TBL and USF, respectively, but, in the vicinity of the edge, there was a multi-structure region (MSR), where the turbulence structure was strongly non-canonical. The dissipation parameter in the MSR was larger than in the TBL and USF and inversely proportional to the local turbulence Reynolds number. The entire flow contained horseshoe-shaped coherent structures, the properties of which, however, were different within the TBL, the MSR and the USF.

INTRODUCTION

Research on turbulence has, to a great extent, focussed on *canonical flows*, which are geometrically simple and reproducible in the laboratory. These include, among others, grid-generated turbulence (GT), uniformly sheared flows (USF) and two dimensional turbulent boundary layers (TBL). Canonical flows themselves are a very small subset of turbulent flows, but they retain some universal features of turbulence. The vast majority of turbulent flows in natural and industrial systems are non-canonical. Because of the diversity and possible complexity of strongly non-canonical flows, information collected for one such flow is rather unlikely to apply to many others. For this reason, a meaningful strategy for expanding our understanding of turbulence seems to be to examine flows with specially designed, mildly non-canonical features. One such example would be a canonical flow that is distorted by an external device or mechanism, which may eventually fade away or be removed. Another example would be the interaction region between two canonical flows. Such flows, either in their entirety or in limited regions, would have non-canonical structures, which are the results of more than one distinct turbulence generation mechanisms; they have recently been referred to as *multi-structure turbulence* (Nedić & Tavoularis, 2018).

TBL are the most intensely researched turbulent flow. In the majority of laboratory studies, the TBL was bounded by a nominally uniform, laminar free stream, in which case the TBL would have a canonical structure. In a few studies, TBL were interacting with a free stream that had some weak, decaying, nearly isotropic turbulence, generated by an upstream grid (Charnay *et al.*, 1971; Evans, 1974; Meier & Kreplin, 1980; Hoffmann *et al.*, 1989). Liangwei & Hoffmann (1988) investigated TBL in free streams with decaying, anisotropic turbulence, generated by bars of different diameters, and concluded that both anisotropic and isotropic free stream turbulence had comparable effects on the boundary layer thickness and the skin friction. More recently, Sakai *et al.* (2013) examined a TBL interacting with the wake of a cylinder in the free stream and found that the inner layer mean flow velocity profile was not altered by the wake, but the intensity of the turbulence decreased. The TBL studied by all these authors would have a multi-structure region, but the deviation from the canonical structure would have vanished as free-stream turbulence decayed. In contrast to such flows, turbulence in USF not only does not decay downstream, but actually becomes intensified, as the result of an active turbulence production mechanism.

Although turbulence is generated by the mean shear in both TBL and USF and there are structural similarities between outer TBL and USF (*e.g.*, comparable Reynolds stress anisotropy levels), there are also some significant differences: a) in TBL, mean shear is produced by friction with the wall, whereas, in USF, mean shear is imposed in the absence of a wall; b) in TBL, the wall also imposes a kinematic constraint, which is absent in USF; c) TBL are separated from the free stream by a thin interface, whereas USF are ideally unbounded in all directions; d) the turbulence in TBL is inhomogeneous, whereas, in USF, turbulence is ideally homogeneous on planes normal to the flow direction; and e) in both TBL and USF, the dominant coherent structures are horseshoe- (or hairpin-)shaped vortices, grouped in packets (Adrian, 2007; Vanderwel & Tavoularis, 2011), but with the difference that the orientation of these structures is constrained by the wall in TBL

but unconstrained in USF. In view of these considerations, the interaction region between a TBL and a uniformly sheared, highly turbulent free stream evolving in parallel seems to be a promising environment for the study of multi-structure turbulence, which is the product of two distinct, persisting and canonical turbulence generation mechanisms. An important point of interest would be to examine how the coherent structures that are generated in a TBL interact with those generated in a USF in the multi-structure region between the two flows. The only relevant previous study is the one by Kislich-Lemyre (2003), which investigated how the large-scale structure of USF was distorted by a solid wall, which was stationary or moving in the same or opposite direction to the flow. When the wall moved faster than the flow, a region of low or zero shear was detected between the wall boundary layer and the free stream USF. Distinct coherent structures were observed on the two sides of this region, which is a region of multi-structure turbulence. Unfortunately, the documentation of this study has been mostly qualitative.

Turbulence theories and models require the use of a length scale and a time scale (or, equivalently, a velocity scale), which characterise the dominant motions and by which one can scale the various statistical properties that appear in the governing equations. An obvious choice for a velocity scale is the square root of the turbulent kinetic energy per unit mass k. A suitable internal length scale is the integral length scale L, which characterises the energy containing motions. The use of the integral length scale L in the analysis is problematic, because the definition of this scale requires consideration of spatial variations of turbulent motions, namely, information which is not contained in the single-point differential equations that describe local turbulent motions. Therefore, there is a need to define a length scale in terms of local variables, namely variables that are contained in the single-point turbulence equations. Besides k and other variables, these equations contain the turbulent kinetic energy dissipation rate per unit mass ε. Although mechanical kinetic energy is dissipated to heat by very small "eddies", there is consensus that the turbulent kinetic energy dissipation rate per unit mass ε is set by the energy containing motions. These motions set the rate by which kinetic energy that is produced at large scales is fed successively to smaller eddies, following the *energy cascade process*, until it reaches the smallest eddies, where it is dissipated. It follows that a *surrogate length scale* $\mathscr{L}$ of the energy containing eddies can be defined by dimensional analysis, namely, by multiplying appropriate powers of k and ε. This provides the result

$$\mathscr{L} \propto k^{3/2}/\varepsilon \,. \tag{1}$$

With the introduction of $\mathscr{L}$, the turbulence scaling issue is reduced to establishing a relationship between L and $\mathscr{L}$, or equivalently, to setting the value of the (dimensionless) *dissipation parameter*

$$C_\varepsilon \propto \frac{\varepsilon L}{k^{3/2}} \propto \frac{L}{\mathscr{L}} \,, \tag{2}$$

where the proportionality coefficient is of order one, but has been given different numerical values by different authors, depending on how k and ε were estimated. A cornerstone assumption of turbulence theories and models is that $C_\varepsilon \approx$ const.. This assumption has been shown to hold approximately for extensive regions of many canonical flows, in which various turbulence properties evolve in a commensurate manner. Nevertheless, there is also a growing body of evidence contradicting this hypothesis in both upstream regions of canonical turbulence and in multi-structure turbulence (Vassilicos, 2015; Nedić *et al.*, 2017; Nedić & Tavoularis, 2018). Testing this hypothesis in the multi-structure region between a TBL and a USF and understanding the relationship among these scales and other flow properties would be of value in explaining the limitations and failures of current turbulence models and in developing improved ones.

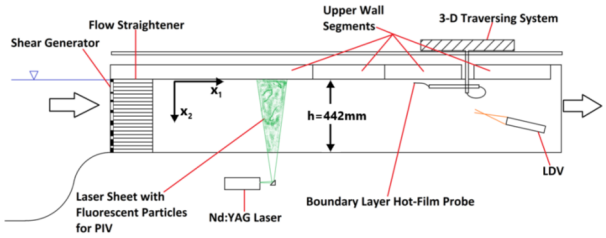

Figure 1. Sketch of the flow facility and instrumentation.

The general goal of this research is to enlarge the available documentation on multi-structure turbulence, particularly one that pertains to TBL. The specific goal is to document experimentally the turbulence in a TBL that is bounded by a highly turbulent, uniformly sheared free stream that has a mean shear opposite in direction to the one inside the TBL. Extensive measurements in such flows were obtained using hot-film anemometry, laser Doppler velocimetry and particle image velocimetry. Measurements include transverse profiles of the mean velocity, the Reynolds stresses, the integral length scales, and the Taylor and Kolmogorov microscales from which it was possible to calculate the local mean shear, the turbulence anisotropies, the turbulent kinetic energy and its dissipation rate, the turbulence Reynolds number Re_λ and the dissipation parameter. Of primary interest in this work is to characterise the behaviour of the dissipation parameter within the multi-structure region and its relationship to Re_λ and to compare the statistical properties of coherent structures in USF, the TBL and the multi-structure region.

APPARATUS AND MEASUREMENT PROCEDURES

The experiments were performed in a recirculating water tunnel, having an enclosed test section with a width of 560 mm, a height $h = 442$ mm and a length of roughly 4.1 m. USF was created by a shear generator, which was a perforated plate with linearly varying solidity, followed by a flow separator, which was a set or parallel plates and acted as a flow straightener, as well as imposing an initial integral length scale uniformity. The examined TBL evolved along the upper wall. A sketch of the experimental setup is shown in Fig. 1 and details have been presented by Livingston (2020).

Vertical profiles of the mean velocity, the Reynolds stresses and the integral length scale were obtained with a two-component, frequency-shifted, laser Doppler velocimeter (LDV - Dantec Dynamics, Skovlunde, Denmark). The lens used with the laser head had a focal length of 243 mm, which produced a measurement volume in the water with approximate dimensions $0.1 \times 0.1 \times 2.0$ mm. The flow was seeded with fused, borosilicate, hollow, glass beads (Potters Industries LLC, Valley Forge, USA), with a density of $1{,}100 \pm 50$ kg/m^3 and an average size of 10 μm. The LDV head was mounted

on the side of the test section on three stacked traverses, which allowed traversing in three mutually perpendicular directions. Measurements were taken on the vertical centreplane of the test section. For turbulence measurements, the streamwise U_1 and vertical U_2 velocity components were measured in coincident burst mode. To take measurements close to the upper wall (within 16 mm), the beams measuring the vertical component were blocked and only the streamwise component was measured. Measurements of each USF profile were made at 33 streamwise locations, at each of which 5000 samples were recorded, typically during 140 s. For measurements near the edge of the boundary layer, 10000 samples were recorded over a time between 48 and 770 s (average of 235 s), which was at least 100 times greater than the local integral time scale. At the two streamwise positions of main interest, $x_1/h = 5.1$ and 6.5, additional one-dimensional measurements were taken that included at least 20000 samples and on average extended for over 360 s, as well as additional two-dimensional data that included 10000 samples and took 180 s on average.

Because the data rate of the LDV system was insufficient to measure accurately the temporal derivative of the velocity, from which one can estimate the Taylor microscale and the dissipation rate, the Taylor microscale was measured directly with the use of a hot film probe (Dantec Dynamics, Model 55R15), which had a 2 μm nickel film on a quartz fibre that was 70 μm in diameter and 1.25 mm long and was of the boundary layer type, so that the sensor could be positioned close to the wall. The hot-film probe was inserted in the test section from the top using waterproof parts and could be traversed in all three directions. The hot-film signal was sampled at a rate of 800 Hz over a 35 s interval, which is at least 100 times the typical integral time scale. Ensemble averaging was performed over 20 of these records at each location. The hot-film signal was low-pass filtered by two double-pole, low-pass filters in series, with the first filter cut-off frequency set to 380 Hz and the second one set to 1.4 kHz. After the voltage signal was recorded and corrected for temperature differences, it was further low-pass filtered by a digital filter with a cut-off frequency that was 2.1 times the local Kolmogorov frequency to prevent aliasing. Attempts to calibrate the hot-film against the LDV demonstrated the presence of a significant and non-repeatable signal drift. This drift is attributed to changes in the thermal resistance of the hot-film surface, as a result of deposits on this surface, which may build up or be removed by the stream. Drift of hot-films immersed in water is well known to users, but there is no effective way to eliminate it or correct for it. Thus, the hot-film measurements were unsuitable for measuring the mean velocity, the streamwise turbulent stress or the streamwise component of the dissipation rate, from which the total dissipation rate can be estimated under the assumption of local isotropy. To circumvent this problem, we devised a procedure by which we measured directly the Taylor microscale from the mean-free, hot-film voltage fluctuations e, even in the presence of drift, as (Livingston, 2020)

$$\lambda \approx \overline{U}_1 \sqrt{\overline{e^2}/\overline{(de/dt)^2}}\,, \tag{3}$$

where the mean velocity $\overline{U}_1$ at the same location was obtained with the LDV system. Equation 3 is only valid under two assumptions: first, that the velocity fluctuations are small compared to the mean local velocity and, second, that the time interval of samples from which the Taylor microscale was determined was sufficiently short for voltage drift to be negligible. Both assumptions were satisfied fairly well by the present conditions. The derivative $\overline{(de/dt)^2}$ was calculated by extrapolating corresponding finite differences to a zero time lag.

Velocity maps on horizontal and vertical planes were constructed with the use of a planar particle image velocimetry system (PPIV, or simply PIV - LaVision Inc., Ypsilanti, USA). The same particles that were used for the LDV method were also serving as tracers for the PIV method. The frequency at which measurements were taken was 7.23 Hz. PIV images were taken in two planes of measurement, the vertical centreplane (x_1,x_2) and the horizontal plane (x_1,x_3). For the measurements in the vertical plane, the laser was positioned underneath the test section and the laser sheet was reflected upwards by a mirror. The camera was attached to a three-dimensional side traverse, which allowed the light sheet to be in focus regardless of its spanwise plane position. The size and location of the images were determined from images of a fine ruler that was inserted on the focal plane of the camera. To take measurements in the horizontal plane, the laser was positioned on the side of the test section, resting on wooden structures with different heights, and a mirror reflected the light sheet into the test section. The camera was setup on a tripod underneath the test section facing upwards. Before determining the vector fields from image pairs, the images were preprocessed. A sliding background was subtracted from each image with a scale between 256 and 512 pixels and the particle intensities were normalised with a scale between one and four pixels. An algorithmic mask was applied to remove any dead pixels in the camera photodiode array or overexposed regions in the image. Each image was processed in an initial pass on 128×128 pixel squares with a 50% overlap and in a second pass on 32×32 pixel squares. The local planar velocity magnitude and direction were determined from the particle displacement that corresponded to the maximum correlation between matched pairs of particle images and the time difference between the two images. Post-processing consisted of deleting values that were significantly different from neighbouring ones and removing sections of the resulting vector field, where the vector density was relatively low. Vectors that exceeded the range of expected velocity were also removed and replaced by interpolated values to fill-in sections of the vector field that were sparse. The edge regions of images were discarded to prevent the final results from being influenced by edge effects.

The process of identifying vortices on PIV vector maps was the same as the one that has been described in detail by Vanderwel & Tavoularis (2011). It is based on the swirling strength, a scalar parameter, the value of which distinguishes discrete vortices from a background flow with mean vorticity. A vortex was assumed to be present, when the swirling strength exceeded a specified threshold value. Regions of the velocity map with sufficiently large swirling strength were fitted with an ellipse, using a minimum volume ellipse function. The orientations of the ellipse axes were used to determine the orientation of the vortex axis. Counter-rotating vortex pairs, which were understood to be the legs of horseshoe-shaped vortices, were identified with the use of a second algorithm.

RESULTS AND DISCUSSION

1 The USF as a free stream

Mean velocity profiles, measured at different streamwise locations, demonstrated that, away from the walls, the mean shear was approximately constant ($d\overline{U}_1/dx_2 \approx 0.41$ s^{-1}, for $1.4 < x_1/h < 8$), so that the "free stream" was indeed a USF. As the TBL on the top wall evolved streamwise, it encroached into the USF, altering the USF mean profile in an increas-

ingly larger region. The shear parameter, based on an average centreline velocity $\overline{U}_{1c} \approx 0.13$ m/s at $x_2/h = 0.5$, was $\beta = (1/\overline{U}_{1c})(d\overline{U}_1/dx_2) \approx 2.9\ \mathrm{m}^{-1}$. Profiles of the streamwise velocity variance at different streamwise locations demonstrated that the turbulence in the USF was approximately homogeneous on a transverse plane, with a level of inhomogeneity that was comparable to those observed in previous USF studies in the same facility (Kislich-Lemyre, 2003; Vanderwel & Tavoularis, 2011). Moreover, the turbulence that was generated by the flow separator decayed in the region $x_1/h \leq 4$, but grew exponentially further downstream, following the well-established USF exponential growth law, *e.g.*, $\overline{u_1^2}/\overline{U}_{1c}^2 \propto e^{0.1\beta x_1}$. In summary, the present results indicate that the free stream was a conventional USF, and so one may use previous findings about its structure.

2 Mean velocity profiles and boundary layer thicknesses

Figure 2 shows vertical profiles of the mean velocity $\overline{U}_1$. From fitted high-order polynomials, we determined the maximum velocity $\overline{U}_{1max}$ and the corresponding distance δ from the wall, to which we will refer as the boundary layer thickness. When plotted *vs.* x_2/δ, most mean velocity profiles nearly collapsed, showing a fair degree of self-similarity of the outer boundary layer. The notable exception was the profile that was closest to the origin ($x_1/h = 1.17$), which was not as developed as the others. Moreover, the farthest away ($x_1/h = 6.5$) profile was also slightly different from the others, which may indicate that other influences in the test section were starting to build up. For $x_2 > \delta$, $\overline{U}_1$ decreased approximately linearly, approaching a canonical USF. The TBL encroached into the USF, such that $\overline{U}_{1max} \approx$ const., whereas $\delta \propto (x_1 + 5.4h)^{0.8}$. Although the mean velocity profile in the inner TBL did not match well the canonical 1/7th power law, the growth rates of the physical and momentum boundary layer thicknesses were close to those in canonical TBL and so the corresponding Reynolds numbers also grew at nearly canonical rates, namely, as $\mathrm{Re}_x = x_1\overline{U}_{1max}/\nu \propto x_1$ and $\mathrm{Re}_\delta = \delta\overline{U}_{1max}/\nu \approx 2600(x_1/h + 5.7)^{0.8}$. The momentum integral thickness θ was computed by integrating the mean velocity profiles in the region $0 < x_2 \leq \delta$. Excluding the values at the two ends of the measurement range, $\theta/\delta \approx 0.092$, which is only slightly lower than the canonical value of 0.094. For rough purposes, and with some reservation for the furthest downstream location, one may approximate the momentum thickness Reynolds number as $\mathrm{Re}_\theta = \theta\overline{U}_{1max}/\nu \approx 240(x_1/h + 5.7)^{0.8}$, with a representative value of 1600 at $x_1/h = 5.0$.

3 Turbulence properties

Profiles of turbulence properties at two streamwise locations are shown in Fig. 3. The C_ε profile clearly shows the presence of three regions: an essentially canonical inner half of a TBL (to be referred to heareafter as simply TBL), for $0 \leq x_2/\delta \lesssim 0.5$; an essentially canonical USF, for $x_2/\delta \gtrsim 2.2$ at $x_1/h = 5.1$ and $x_2/\delta \gtrsim 1.7$ at $x_1/h = 6.5$; and an intermediate, non-canonical, MSR. The mean shear in the MSR was lower than outside it and the turbulence anisotropy was lower in the MSR as well. The turbulent shear stress profile was consistent with gradient transport. The integral length scales in the outer TBL and in the USF happened to have comparable values and so this scale did not change measurably in the MSR. The Taylor and Kolmogorov microscales (not shown here) exhibited nearly canonical trends outside the MSR but had distinct

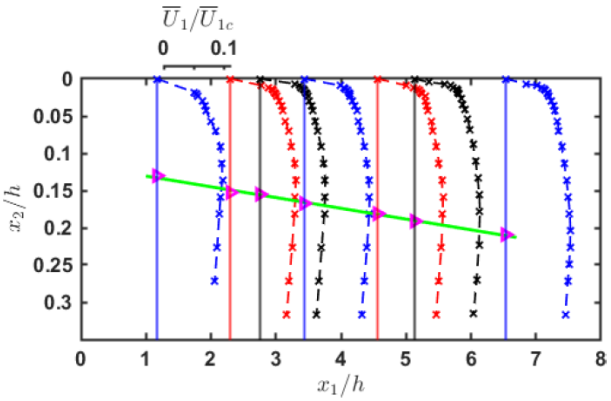

Figure 2. Streamwise evolutions of the mean velocity profiles and the physical boundary layer thickness.

patterns within the MSR.

An important observation is that the dissipation parameter had significantly larger values within the MSR than outside it, where it essentially matched values in the corresponding canonical flows. A second important observation is that the turbulence Reynolds number inside the MSR was lower than outside it. In fact, as shown in Fig. 4, across the MSR, C_ε was roughly inversely proportional to the local Re_λ, whereas, in contrast, in the TBL and the USF, there was no obvious correlation between C_ε and Re_λ.

4 Comparisons with measurements in a boundary layer with a uniform free stream

The profiles of the mean velocity and the streamwise Reynolds stress across a TBL on the upper wall in the present water tunnel in the absence of USF were measured at $x_1/h = 5.1$ with the LDV system after the shear generator and flow separator were removed. The values of some basic properties of this TBL, together with corresponding values in the presence of USF shown within parentheses, were as follows: $\overline{U}_{1\mathrm{max}} = 0.14$ (0.20) m/s; $\delta = 0.080$ (0.084) m; $\mathrm{Re}_x = 330{,}000$ (470,000); and $\mathrm{Re}_\theta = 1{,}000$ (1,600). Differences between the two normalised mean velocity profiles within the TBL are within the measurement uncertainty, which was more significant near the wall. Neither profile could be fitted well by the 1/7th law, but both profiles were, at least partially, fairly close to a 1/6th law. These results show that the presence of shear in the free stream has no measurable effect on the mean velocity profile inside the TBL. It should be mentioned, however, that, even in the absence of USF, the free stream contained a significant level of disturbances (nearly 2%). It was also found that the turbulence in the inner TBL ($x_2/\delta \lesssim 0.2$) was not affected visibly by the presence of USF, whereas, in the outer TBL ($0.2 \lesssim x_2/\delta < 1$), the local turbulence was stronger in the presence of USF, as the result of both the overall higher turbulence level in the USF and the penetration of coherent structures from the USF into the TBL.

5 Coherent structures

Figure 5 shows representative instantaneous velocity maps obtained with the PIV system on the vertical centreplane of the test section at two different elevations and two streamwise stations. These maps revealed the presence of vortices, which were interpreted as mostly cross-sections of heads of horseshoe-shaped coherent structures. It was hypothesised that

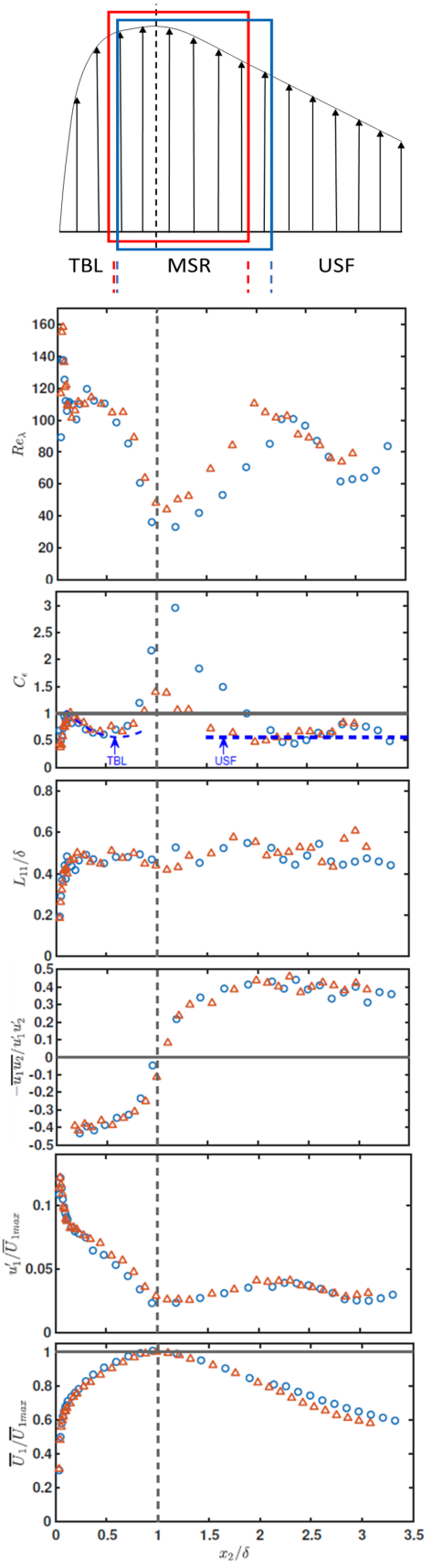

Figure 3. Profiles of turbulence properties at $x_1/h = 5.1$ (blue circles) and 6.5 (red triangles); in the C_ε plot, the dashed lines mark fits to measurements in a canonical TBL (Nedić *et al.*, 2017) and a USF (Nedić & Tavoularis, 2016).

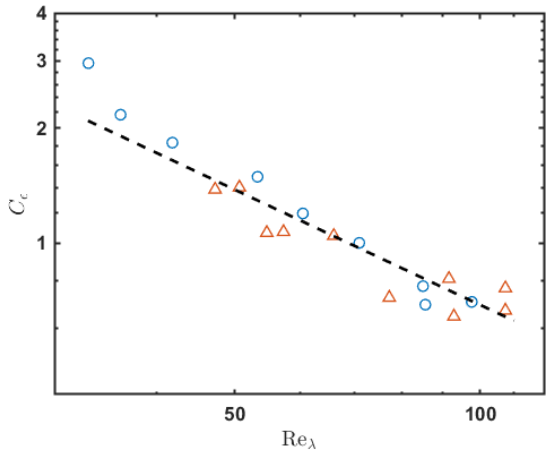

Figure 4. The dissipation parameter *vs.* the turbulence Reynolds number in the multistructure region at $x_1/h = 5.1$ (blue circles) and 6.5 (red triangles); the dashed line is a fitted relationship of the type $C_\varepsilon \propto \mathrm{Re}_\lambda{}^{-1}$.

counter-clockwise (CCW) vortices were produced by wall-generated mean shear, whereas clockwise (CW) vortices were produced by free shear in the USF. Both vortex types were observed across the flow, but one may confirm qualitatively that the majority of vortices well inside the TBL are CCW, those well inside the USF are CW, and those in the multi-structure region are mixed. These images also show flood maps of the velocity magnitude. As shown previously for both canonical TBL (de Silva *et al.*, 2016) and undistorted USF (Vanderwel & Tavoularis, 2016), the flow velocity field does not change continuously across the test section, but consists of zones of nearly uniform velocity. The vortices tend to cluster at the boundary between such zones, in conformity with the literature.

Instantaneous velocity maps on horizontal planes at different distances from the wall (see Fig. 6) revealed the presence of many vortices, several counter-rotating pairs of which could be matched and interpreted as cross-sections of the legs of horseshoe structures. Vortex packets were observed, straddling low-speed or high-speed streaks, which are the result of vertical flow motion induced by the legs of a vortex. Both upright and inverted (Vanderwel & Tavoularis, 2011) horseshoe vortices were identified in all of the horizontal planes, but the images could not discriminate between vortices produced by the two shear mechanisms. The density of horseshoes was greater within the TBL than in the MSR and the USF. In all regions, however, the densities of CW and CCW vortices were nearly the same and the densities of upright and inverted horseshoes were also roughly the same. The latter observation conforms with the literature as far as USF is concerned (Vanderwel & Tavoularis, 2011), but seems to be a novel one for TBL. Another piece of information that was extracted from the images was the average inclination of the horseshoes with respect to the horizontal plane. This property was determined from the aspect ratio of the ellipses, under the assumption that each ellipse is a cross-section of a cylindrical vortex. Our analysis indicated that this inclination spanned a wide range, but, on the average, was roughly 55° at all four elevations. This value is somewhat larger than values reported in the TBL and USF literature.

The distance between vortices that do not belong to the same packet was comparable to the integral length scale. The distance between the legs of horseshoes was roughly equal to twice the Taylor microscale. Because of the random yaw of

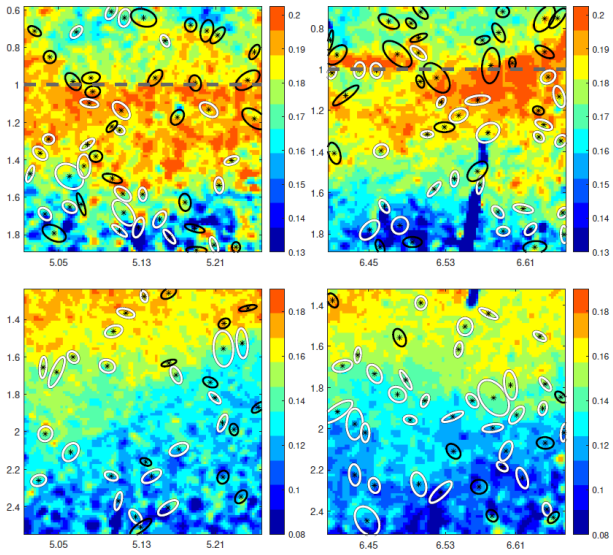

Figure 5. Representative instantaneous, vertical, velocity maps at two different elevations (top and bottom rows) and $x_1/h \approx 5.1$ (left column) and 6.5 (right column); numbers on the ordinate denote x_2/δ and numbers on the abscissa denote x_1/h; legends (specific to each image) describe the velocity magnitude in m/s; the physical scales of both axes are the same; ellipses mark areas with relatively large swirl, which are interpreted to be cross sections of mostly vortex heads; white ellipse contours indicate clockwise rotation and black ones indicate counter-clockwise rotation.

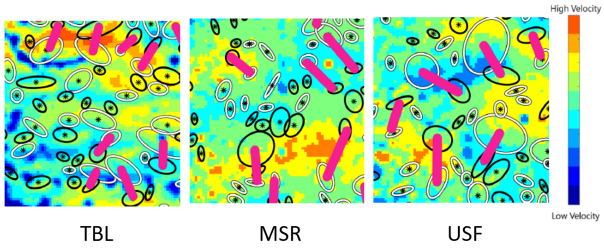

Figure 6. Representative instantaneous, horizontal, velocity maps showing vortex pairs in the three regions; ellipses mark areas with relatively large swirl, which are interpreted to be cross sections of mostly vortex legs; white ellipse contours indicate clockwise rotation and black ones indicate counter-clockwise rotation; hand-drawn red lines connect the axes of selected vortex pairs, deemed to be the legs of horseshoes.

the vortices, the shortest distance between their legs would be smaller than the distance between the axes of their intersections with the horizontal plane, thus roughly validating Tennekes' postulate that the distance between vortex legs is comparable to the Taylor microscale (Tennekes, 1968). The diameter of vortices was an order of magnitude larger than the Kolmogorov microscale, contradicting Tennekes' second postulate that the diameter of each vortex is comparable to the Kolmogorov microscale.

CONCLUSIONS

A turbulent boundary layer was generated in the laboratory with a highly turbulent free stream that consisted of a uniformly sheared flow with a mean shear direction that was opposite to the direction of wall-generated shear. An intermediate, distinct, multi-structure region was identified, as having non-canonical properties and within which the dissipation parameter was significantly larger than elsewhere and inversely proportional to the local turbulence Reynolds number. Horseshoe vortices were the dominant coherent structures in the entire flow, but their characteristics were distinct in each of the three flow regions.

Financial support was provided by the Natural Sciences and Engineering Research Council of Canada.

REFERENCES

Adrian, R. J. 2007 Hairpin vortex organization in wall turbulence. *Phys. Fluids* **19** (4), 041301 (16pp).

Charnay, G., Comte-Bellot, G. & Mathieu, J. 1971 Development of a turbulent boundary layer on a flat plate. In *Turbulent Shear Flows*, pp. 27.1–27.10. Technical Editing and Reproduction Ltd.

Evans, R. L. 1974 Free-stream turbulence effects on the turbulent boundary layer. *Aeronautical Research Council Current Papers No. 1282* .

Hoffmann, J. A., Kassir, S. M. & Larwood, S. M. 1989 The influence of free-stream turbulence on turbulent boundary layers with mild adverse pressure gradients. *Tech. Rep.* 177520. NASA, Ames Research Center.

Kislich-Lemyre, B. C. 2003 The large-scale structure of uniformly sheared turbulence and its distortion by a solid wall at rest or in motion. PhD thesis, University of Ottawa.

Liangwei, Fang & Hoffmann, J.A. 1988 Effects of anisotropic free-stream turbulence on turbulent boundary layer behavior. In *Frontiers of Fluid Mechanics* (ed. Shen Yuan), pp. 56 – 61. Pergamon.

Livingston, C. 2020 Multi-structure turbulence in a boundary layer with a uniformly sheared free stream. Master's thesis, University of Ottawa.

Meier, H. U. & Kreplin, H.-P. 1980 Influence of freestream turbulence on boundary-layer development. *AIAA J.* **18** (1), 11–15.

Nedić, J. & Tavoularis, S. 2016 Energy dissipation scaling in uniformly sheared turbulence. *Phys. Rev. E* **93** (3).

Nedić, J. & Tavoularis, S. 2018 A case study of multi-structure turbulence: Uniformly sheared flow distorted by a grid. *Int. J. Heat Fluid Flow* **72**, 233–242.

Nedić, J., Tavoularis, S. & Marusic, I. 2017 Dissipation scaling in constant-pressure turbulent boundary layers. *Phys. Rev. Fluids* **2** (3), 032601 (7pp).

Sakai, Y., Hiruta, K., Nagata, K., Suzuki, H. & Terashima, O. 2013 Effects of the cylinder wake in a freestream on statistical properties of a turbulent boundary layer. *Trans. JSME (in Japanese)* **79** (799), 64–76.

de Silva, C. M., Hutchins, N. & Marusic, I. 2016 Uniform momentum zones in turbulent boundary layers. *J. Fluid Mech.* **786**, 309–331.

Tennekes, H. 1968 Simple model for the small-scale structure of turbulence. *Phys. Fluids* **11** (3), 669–671.

Vanderwel, C. & Tavoularis, S. 2011 Coherent structures in uniformly sheared turbulent flow. *J. Fluid Mech.* **689**, 434–464.

Vanderwel, C. & Tavoularis, S. 2016 Scalar dispersion by coherent structures in uniformly sheared flow generated in a water tunnel. *J. Turbul.* **17** (7), 633–650.

Vassilicos, J. C. 2015 Dissipation in turbulent flows. *Annu. Rev. Fluid Mech.* **47** (1), 95–114.